Phase diagram of a flexible two-dimensional material

D. R. Saykin,[1] V. Yu. Kachorovskii,[2,3] and I. S. Burmistrov[4,5]

[1]*Department of Physics, Stanford University, Stanford, California 94305, USA*
[2]*Ioffe Institute, Polytechnicheskaya 26, 194021 St. Petersburg, Russia*
[3]*Institute for Quantum Materials and Technologies, Karlsruhe Institute of Technology, 76021 Karlsruhe, Germany*
[4]*L. D. Landau Institute for Theoretical Physics, Semenova 1-a, 142432 Chernogolovka, Russia*
[5]*Laboratory for Condensed Matter Physics, National Research University Higher School of Economics, 101000 Moscow, Russia*

(Received 6 March 2020; revised 29 July 2020; accepted 1 October 2020; published 19 October 2020)

Transport and elastic properties of freestanding two-dimensional materials are determined by competition between dynamical and quenched out-of-plane deformations, i.e., between flexural phonons and ripples, respectively. They both tend to crumple the system by overcoming the strong anharmonicity which stabilizes the flat phases. Despite active research, it still remains unclear whether the rippled phase exists in the thermodynamic limit or is destroyed by thermal out-of-plane fluctuations. We demonstrate that a sufficiently strong short-range disorder stabilizes ripples, whereas in the case of a weak disorder the thermal flexural fluctuations dominate in the thermodynamic limit. Therefore the phase diagram of a flexible two-dimensional material with a quenched short-range disorder has four distinct phases. These phases have drastically different elastic and transport properties that are of crucial importance for the emergent field of flexible nanoelectronics.

DOI: 10.1103/PhysRevResearch.2.043099

I. INTRODUCTION

The discovery of graphene [1–3] and other flexible two-dimensional (2D) materials [4] is an outstanding breakthrough in condensed-matter physics. Such materials have the out-of-plane bending degree of freedom, which governs a number of amazing physical phenomena [5–14], explored in the emergent field of *flexible nanoelectronics* [14–18]. A peculiarity of this field is the competition of dynamical flexural phonons, which dominate in clean systems and static out-of-plane deformations, called ripples, induced by a quenched disorder.

Despite great effort, the basic physics behind flexible nanoelectronics, which is based on a synergy of electrical, optical, and elastic properties of flexible 2D materials, is still not well understood. Even the temperature dependence of conductivity, which should be essentially different in dynamical and static regimes, is not established. The key unsolved question is the phase diagram of a flexible 2D material that accounts for competition between flexural phonons and ripples in the presence of strong anharmonicity which prevents crumpling [19–25].

In this paper, we report the phase diagram of a flexible 2D material with a quenched short-range disorder. Our main results are illustrated in Fig. 1 and can be formulated as follows:

(i) There are four distinct phases: clean or rippled flat ones and clean or rippled crumpled ones. They are split up by two separatrices, which correspond to the crumpling (red curve) and rippling (blue line) transitions. The transition lines cross each other in the fully unstable, *multicritical* fixed point M.

(ii) There is a stable fixed point F corresponding simultaneously to the clean and rippled flat phases. The coexistence of two distinct flat phases at the single fixed point reflects noncommutativity of limits of vanishing thermal and rippling fluctuations caused by *singularity* in the corresponding renormalization group (RG) equations; see Eq. (9) below.

II. CRITICAL ELASTICITY OF MEMBRANES

The problem addressed in this paper has a close connection with the critical elasticity of 2D crystalline membranes. It dates back to the seminal paper by Nelson and Peliti [19], in which the idea of crumpling transition, i.e., the transition between flat and crumpled phases, was put forward. The thermal out-of-plane fluctuations tend to crumple the membrane. In contrast, the long-range interactions between flexural phonons, i.e., anharmonic effects, "iron" the membrane and stabilize the flat phase. As a result of such competition, flat and crumpled phases can exist in a clean crystalline membrane. A more detailed analysis of the crumpled transition and the critical elasticity of clean membranes has been developed in Refs. [20–25]. Ripples caused by imperfection of the crystal lattice act similarly to flexural phonons and also tend to crumple the membrane as was predicted a long time ago [26–30].

The importance of competition between flexural phonons and ripples is most evident in freestanding graphene. Indeed, the effect of the thermal fluctuations is controlled by the ratio of temperature T and the bending rigidity $\varkappa_0$. In a clean membrane the crumpling transition occurs at $T/\varkappa_0 \sim 1$. In graphene, $\varkappa_0 \sim 1$ eV, so that the thermal fluctuations alone are

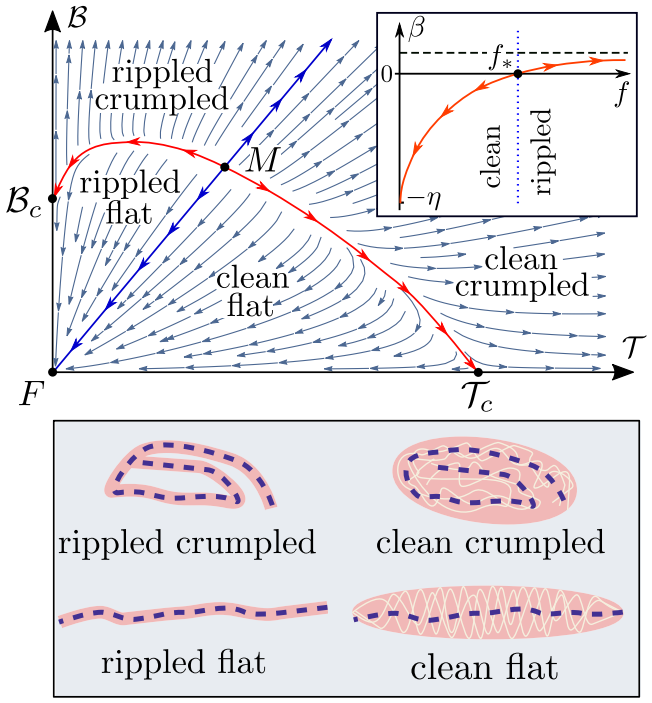

FIG. 1. Sketch of the phase diagram and side views of a membrane. $\mathcal{B}$ is the rescaled disorder strength and $\mathcal{T}$ is the amplitude of thermal fluctuations; see text below Eq. (2). The solid red curve corresponds to the crumpling transition. The solid blue line is the rippling-transition line, separating disordered and clean phases. The fully unstable (multicritical) point is marked by M. Two flat phases (clean and disordered) coexist in the stable singular fixed point F reflecting noncommutativity of limits of vanishing thermal and rippling fluctuations. The arrows mark direction of RG flow towards the infrared. Pink shaded regions are traces of the membrane profiles due to dynamical fluctuations. Inset: The sketch of the RG flow for $f = \mathcal{B}/\mathcal{T}$.

not enough to crumple it. At the same time, recent numerical simulations of disordered graphene clearly indicate the crumpling transition [31]. Additional evidence for the importance of disorder in graphene is provided by recent experimental measurements of anomalous Hooke's law [32,33]. The measured scaling exponent was substantially different from the one known from numerical simulations of a clean membrane [34]. These findings imply the existence of the rippled phase with properties distinct from the clean flat phase.

Previous theoretical studies of disordered 2D materials [29,30] predict the existence of the rippled flat phase at exactly zero temperature, $T = 0$, and instability with respect to the thermal fluctuations (similar results have been obtained for disordered membranes of dimension $D = 4 - \epsilon$ [26–28]). This conclusion implies the absence of the stable rippled phase and, at first glance, contradicts the observations of Refs. [31–34]. Recently, the crumpling transition in disordered freestanding graphene was addressed in Ref. [35]. It was shown that (i) disorder can crumple a membrane in agreement with Ref. [31] and (ii) instability of the rippled phase predicted in Refs. [29,30] develops logarithmically slow, i.e., the marginal $T = 0$ rippled phase controls elastic properties of disordered freestanding graphene for $T \neq 0$ in a wide interval of length scales (see also Ref. [36]) but does not "survive" in the thermodynamic limit even for the case of an ultimate strong disorder. This marginal behavior can manifest itself in experiments on anomalous Hooke's law in graphene [32,33] as was demonstrated in Ref. [37]. Alternatively, observations in Refs. [31–33] could be the manifestation of a stable rippled flat phase at $T \neq 0$. Here, we use the standard model of a disordered membrane and prove that the second scenario is realized.

III. THE MODEL

There are many ways to introduce a disorder experimentally: by bombarding graphene with heavy atoms [38], by fluorination [39], or by creating macroscopical defects, e.g., artificial holes [40]. Theoretically, one classifies disorder with respect to the reflection symmetry related to the top and bottom surfaces of a membrane. An example of disorder which preserves the reflection symmetry is the so-called metric or in-plane disorder. It can arise due to fluctuations in the concentration of impurity atoms. Such short-range disorder is irrelevant at $T \neq 0$ in the thermodynamic limit, i.e., the flat phase remains stable [27,28,35] (for discussion of the special case $T = 0$, see Ref. [41]). Therefore we focus on a random curvature disorder which breaks the reflection symmetry [26,29,30]. Such disorder naturally arises if adatoms are situated on the top or bottom surface only.

We consider a standard model with a large number, d_c, of flexural phonon modes, which allows one to develop controllable perturbation theory in $1/d_c$ [22,42]. In order to determine the phase diagram, it is sufficient to perform $1/d_c$ expansion up to the second order. As was recently demonstrated [43–45], among second-order diagrams there are such that are not accounted for by the so-called self-consistent screening approximation (SCSA) [46], which is frequently discussed as an efficient approximate scheme [36,47]. Our results represent rigorous treatment of anharmonicity in disordered membranes within the second order in $1/d_c$ expansion, which is not accounted for either by SCSA or by other approximative schemes such as the nonperturbative RG approach [48–50]. We show that the finite temperature instability of the rippled phase was an artefact of the first-order approximation in $1/d_c$. Terms of the higher order in $1/d_c$ stabilize the rippled phase and lead to the appearance of the rippling transition (the blue line in Fig. 1).

The membrane's configuration is parametrized with a vector $\boldsymbol{r}(\boldsymbol{x}) \in \mathbb{R}^d$, $\boldsymbol{x} \in \mathbb{R}^D$, where $D = d - d_c$. We introduce stretching factor ξ_0, which characterizes the projective area of a membrane, $\xi_0^2 L^2$, and use vectors $\boldsymbol{u}(\boldsymbol{x}) \in \mathbb{R}^D$ and $\boldsymbol{h}(\boldsymbol{x}) \in \mathbb{R}^{d_c}$ to describe in-plane and out-of-plane displacements: $\boldsymbol{r} = \xi_0 \boldsymbol{x} + \boldsymbol{u} + \boldsymbol{h}$. The energy of the crystalline membrane consists of bending and elastic contributions [19,26,29,30]

$$\mathcal{F} = \int d^2\boldsymbol{x} \left[\frac{\varkappa_0}{2} (\Delta \boldsymbol{h} - \boldsymbol{\beta})^2 + \mu_0 u_{\alpha\beta}^2 + \frac{\lambda_0}{2} u_{\alpha\alpha}^2 \right]. \quad (1)$$

Here μ_0 and λ_0 stand for the Lamé coefficients. The last two terms on the right-hand side of Eq. (1) describe the in-plane elastic energy with the strain tensor $u_{\alpha\beta} = (\partial_\alpha u_\beta + \partial_\beta u_\alpha + \partial_\alpha \boldsymbol{h} \partial_\beta \boldsymbol{h})/2$. Quenched random curvature is added via a zero-mean Gaussian random vector $\boldsymbol{\beta}$ [26,29,30]. The strength

of disorder is controlled by a variance b_0: $\overline{\beta_j(\boldsymbol{x})\beta_k(\boldsymbol{x}')} = b_0\,\delta_{jk}\delta(\boldsymbol{x}-\boldsymbol{x}')$, $j,k=1,\ldots,d_c$.

In the absence of disorder the theory based on Eq. (1) contains an important length scale, the so-called Ginzburg length $L_* \sim \varkappa_0/\sqrt{Y_0 T}$ [24] separating the regime of conventional elasticity, $L \ll L_*$, from the universal scaling regime, $L \gg L_*$. Here, $Y_0 = \frac{4\mu_0(\mu_0+\lambda_0)}{(2\mu_0+\lambda_0)}$ denotes the bare (ultraviolet) value of the 2D Young's modulus. Due to an anharmonic coupling between the in-plane and out-of plane elastic modes, the bending rigidity scales in the universal regime as $\varkappa \propto \varkappa_0(L/L_*)^\eta$, where η is a critical exponent. Although the crumpling transition cannot be observed in a clean graphene, the anomalous power-law scaling of $\varkappa$ leads to highly nontrivial phenomena already verified experimentally, such as anomalous Hooke's law [23,24,32–34,37,51,52], negative thermal expansion coefficient [53–59], power-law scaling with T of the phonon-limited conductivity [60–62], etc.

IV. CRUMPLING TRANSITION AND $1/d_c$ EXPANSION

The stretching factor scales with a membrane size L as [35]

$$d\xi^2/d\ln L = -d_c(\mathcal{T}+\mathcal{B})\xi^2/(4\pi), \quad \xi(L_*) = \xi_0, \qquad (2)$$

where $\mathcal{T} = T/\varkappa\xi^2$ and $\mathcal{B} = b/\xi^2$ are rescaled amplitudes of the thermal and disorder-induced fluctuations, respectively. Here, $\varkappa$ and b are the scale-dependent bending rigidity and disorder variance, respectively. The crumpling transition occurs when $\xi(L)$ turns into zero at a finite length scale, while in the flat phase $\xi(\infty) > 0$. Both the thermal and rippling fluctuations contribute to crumpling of the membrane [cf. Eq. (2)]. There is a dimensionless parameter $f = \mathcal{B}/\mathcal{T} = b\varkappa/T$ that controls the relative strength of the rippling fluctuation in comparison with the flexural phonons. In the clean case, $\mathcal{B} = 0$, the power-law dependence of $\varkappa$ on L results in the crumpling transition occuring at a very high temperature $T_c = 4\pi\eta\varkappa_0/d_c$. In a disordered membrane, scaling of $\mathcal{T}$ and $\mathcal{B}$ is more intricate than a power law. There is a crumpling-transition curve in the plane $(\mathcal{T},\mathcal{B})$ which was found in Ref. [35] by using the first-order expansion over $1/d_c$. Below we demonstrate that the higher-order terms in $1/d_c$ lead to the rippling transition (the blue line in Fig. 1).

Replicating $\boldsymbol{u}$ and $\boldsymbol{h}$ in Eq. (1), integrating over $\boldsymbol{u}$, and averaging the replicated partition function over disorder, we obtain the effective free energy [35]:

$$\mathcal{F}_{\rm dis} = \sum_{a,b=1}^{N}\int\frac{d^2\boldsymbol{k}}{(2\pi)^2}\frac{\varkappa_{ab}\boldsymbol{k}^4}{2}\left(\boldsymbol{h}_{\boldsymbol{k}}^{(a)}\boldsymbol{h}_{-\boldsymbol{k}}^{(b)}\right) + \frac{Y_0}{8}\sum_{a=1}^{N}\int\frac{d^2\boldsymbol{q}}{(2\pi)^2}\left|\int\frac{d^2\boldsymbol{k}}{(2\pi)^2}\frac{[\boldsymbol{k}\times\boldsymbol{q}]^2}{q^2}\left(\boldsymbol{h}_{\boldsymbol{k}+\boldsymbol{q}}^{(a)}\boldsymbol{h}_{-\boldsymbol{k}}^{(a)}\right)\right|^2. \qquad (3)$$

Here, N stands for the number of replicas. We introduced the $N\times N$ matrix $\varkappa_{ab} = \varkappa_0[\delta_{ab} - f_0 J_{ab}]$, where $f_0 = b_0\varkappa_0/T$ and the matrix $\hat{J}$ has all elements equal to unity.

Anharmonicity of flexural phonons results in a renormalization of the parameters of $\mathcal{F}_{\rm dis}$. The necessary information can be extracted from the exact two-point Green's function $\langle h_i^{(a)}(\boldsymbol{k})h_j^{(b)}(-\boldsymbol{k})\rangle \equiv \hat{\boldsymbol{\mathcal{G}}}_{ab}(k)\delta_{ij}$, where the average is with respect to the free energy (3). The quadratic part of $\mathcal{F}_{\rm dis}$ determines the bare Green's function $\hat{\mathcal{G}}_{ab}(k) = T(\delta_{ab} + f_0 J_{ab})/(\varkappa_0 k^4)$. At first, the screening of the interaction between flexural phonons should be taken into account via random-phase approximation (RPA)-type resummation [see Fig. 2(a) and Appendix A]. The screened interaction becomes independent of Y_0 for $q < \tilde{L}_*^{-1} = \sqrt{d_c(1+2f_0)}/L_*$ and behaves as $Y_q \sim q^2/d_c$ in the limit $q \to 0$ [35]. For graphene, $L_* \sim 1 \div 10$ nm. Since $\tilde{L}_* < L_*$, flakes of disordered graphene of realistic size are always in the universal regime. Using the smallness of Y_q, we construct the regular perturbation theory in $1/d_c$ for the self-energy $\hat{\Sigma}$ [see diagrams in Figs. 2(b) and 3], which relates the exact and bare Green's functions: $\hat{\boldsymbol{\mathcal{G}}}^{-1} = \hat{\mathcal{G}}^{-1} - \hat{\Sigma}$.

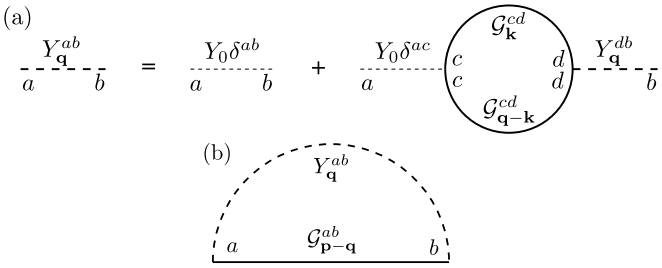

FIG. 2. (a) The equation for the screened interaction. (b) The self-energy correction of the first order in $1/d_c$.

V. RESULTS

The perturbation theory for $\hat{\Sigma}(k)$ has infrared logarithmic divergences as $k \to 0$ (see Appendix B). They can be used to extract the scaling behavior of the theory (see Appendix C),

$$\frac{d\ln\varkappa}{d\ln L} = \eta_\varkappa(f) = \frac{\eta_\varkappa^{(1)}}{d_c} + \frac{\eta_\varkappa^{(2)}}{d_c^2} + \cdots,$$
$$-\frac{d\ln b}{d\ln L} = \eta_b(f) = \frac{\eta_b^{(1)}}{d_c} + \frac{\eta_b^{(2)}}{d_c^2} + \cdots. \qquad (4)$$

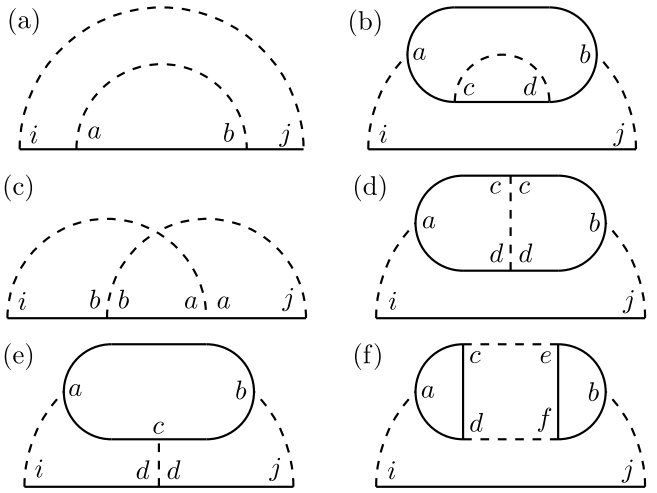

FIG. 3. Diagrams for the self-energy corrections in the second order in $1/d_c$. Diagrams (a) and (b) are included in the SCSA. Diagrams (c)–(f) are not taken into account by the SCSA.

The explicit expressions for $\eta^{(1),(2)}_{\varkappa,b}$ are given as

$$\eta^{(1)}_{\varkappa} = \frac{2(1+3f+f^2)}{(1+2f)^2}, \quad \eta^{(1)}_{b} = \frac{2(2+6f+f^2)}{(1+2f)^2}, \tag{5}$$

$$\begin{aligned}\eta^{(2)}_{\varkappa} = [&73 + 803f + 3550f^2 + 7743f^3 + 7995f^4 + 3046f^5 \\ &+ 265f^6 - 68\zeta(3)(1 + 11f + 49f^2 + 111f^3 + 129f^4 \\ &+ 64f^5 + 9f^6)]/[27(1+2f)^6],\end{aligned} \tag{6}$$

and

$$\begin{aligned}\eta^{(2)}_{b} = [&146 + 1606f + 7217f^2 + 16\,260f^3 + 17\,273f^4 \\ &+ 6466f^5 + 451f^6 - 68\zeta(3)(2 + 22f + 98f^2 \\ &+ 222f^3 + 257f^4 + 122f^5 + 15f^6)]/[27(1+2f)^6].\end{aligned} \tag{7}$$

The RG flow for the theory (3) can be cast in the form of the single-parameter scaling,

$$d\ln f/d\ln L = \beta(f) = \eta_{\varkappa}(f) - \eta_b(f). \tag{8}$$

The function $\beta(f)$ is shown in the inset of Fig. 1. It has three fixed points: 0, ∞, and $f_* \approx 8.5\,d_c$ [63]. The fixed point $f = 0$ is *stable* in the infrared and describes *the clean flat phase*. At $f = 0$ the bending rigidity and disorder variance acquire the power-law scaling, $\varkappa \sim L^{\eta}$ and $b \sim L^{-\eta'}$, where $\eta = \eta_{\varkappa}(0)$ and $\eta' = \eta_b(0)$. They are not independent: $\eta' = 2\eta$. The expansion to the second order in $1/d_c$ yields $\eta \approx \frac{2}{d_c} - \frac{68\zeta(3)-73}{27d_c^2}$ [45]. Both exponents characterize the spatial behavior of two types of roughness correlation functions, $\overline{\langle \delta h(\boldsymbol{x})\delta h(0)\rangle} \sim |\boldsymbol{x}|^{2-\eta}$ and $\overline{\langle h(\boldsymbol{x})\rangle\langle h(0)\rangle} \sim |\boldsymbol{x}|^{2-\eta'}$, where $\delta h(\boldsymbol{x}) = h(\boldsymbol{x}) - \langle h(\boldsymbol{x})\rangle$ and $\langle\cdots\rangle$ stands for the average with respect to $\mathcal{F}$ [36].

The *infrared stable* fixed point at $f = \infty$ describes *the rippled flat phase* (within the expansion of the first order in $1/d_c$ this fixed point was found to be marginally unstable [29,35]). At $f = \infty$ the bending rigidity and the disorder variance have a power-law scaling with momentum, $\varkappa \sim L^{\eta_\infty}$ and $b \sim L^{-\eta'_\infty}$, where $\eta_\infty = \eta_{\varkappa}(\infty)$ and $\eta'_\infty = \eta_b(\infty)$. Within the expansion of the second order in $1/d_c$ we find $\eta_\infty \approx \frac{1}{2d_c} - \frac{612\zeta(3)-265}{1728d_c^2}$ and $\eta'_\infty \approx \eta_\infty - \frac{68\zeta(3)-31}{228d_c^2}$. The fixed point at $f = f_*$ is *unstable* in the infrared and corresponds to *the rippling transition* [64]. This transition is characterized by the divergent correlation length with the exponent $\nu = 1/[f d\beta/df]|_{f=f_*} = \frac{288d_c^2}{68\zeta(3)-31}$.

In order to elucidate the physics of the rippling and crumpling transitions we study the RG flow of $\mathcal{T}$ and $\mathcal{B}$:

$$\begin{aligned}d\ln\mathcal{T}/d\ln L &= d_c(\mathcal{B}+\mathcal{T})/(4\pi) - \eta_{\varkappa}(\mathcal{B}/\mathcal{T}), \\ d\ln\mathcal{B}/d\ln L &= d_c(\mathcal{B}+\mathcal{T})/(4\pi) - \eta_b(\mathcal{B}/\mathcal{T}).\end{aligned} \tag{9}$$

The flow diagram for $\mathcal{B}$ and $\mathcal{T}$ is shown in Fig. 1. There is an *unstable* fixed point at $\mathcal{T}_c = 4\pi\eta/d_c$ and $\mathcal{B} = 0$, corresponding to the crumpling transition due to thermal fluctuations in the absence of disorder. This fixed point controls the transition between the clean flat phase and the clean crumpled phase. The *unstable* fixed point at $\mathcal{T} = 0$ and $\mathcal{B}_c = 4\pi\eta'_\infty/d_c$ corresponds to the disorder-driven crumpling transition [35]. This fixed point controls transition between flat and crumpled rippled phases. Remarkably, both the clean flat phase ($f = 0$) and the rippled flat phase ($f = \infty$) are described by the *single singular infrared stable* fixed point F at $\mathcal{T} = \mathcal{B} = 0$. The singularity at $\mathcal{T} \to 0$ and $\mathcal{B} \to 0$ is clearly seen from the explicit expressions for the functions $\eta_{\varkappa}(\mathcal{B}/\mathcal{T})$ and $\eta_b(\mathcal{B}/\mathcal{T})$; see Eqs. (4)–(7)]. RG equations (9) admit the *multicritical* (more precisely, tetracritical) fixed point M at $\mathcal{T}_* = 4\pi\eta_{\varkappa}(f_*)/[d_c(1+f_*)]$ and $\mathcal{B}_* = f_*\mathcal{T}_*$ (see Fig. 1). This multicritical fixed point has two unstable directions: along the crumpling-transition curve, which demarks flat and crumpled phases, and along the rippling-transition line, $\mathcal{B} = f_*\mathcal{T}$, which splits up clean and rippled phases and connects M and F. The scaling along these two separatrices is controlled by the critical exponents ν and $1/\eta_{\varkappa}(f_*)$, respectively. We emphasize the striking resemblance of our RG flow diagram to the one for the random-bond Ising model [65]. The rippling-transition line corresponds to the so-called Nishimori line [66].

In the course of derivation of RG equations (9) we neglected the term $\partial_\alpha \boldsymbol{u}\partial_\beta \boldsymbol{u}$ in the expression for $u_{\alpha\beta}$. This approximation is justified for $\mathcal{B}, \mathcal{T} \ll 1$ [67]. The terms $\partial_\alpha \boldsymbol{u}\partial_\beta \boldsymbol{u}$ provide additional contributions to Eqs. (9) that are of higher order in powers of $\mathcal{B}$ and $\mathcal{T}$. These terms do not affect the properties of the fixed point F but can result in corrections of higher order in $1/d_c$ to the position of the crumpling-transition line as well as to the critical exponents governing scaling behavior at the fixed points $\mathcal{B}_c$, $\mathcal{T}_c$, and M [67].

VI. DISCUSSION AND CONCLUSION

Our key result is the demonstration of the stabilization of ripples by sufficiently strong disorder. More precisely, for $\mathcal{T} < \mathcal{T}_*$ (see Fig. 1), when disorder is increased the membrane first undergoes transition corresponding to the stabilization of ripples, and as disorder is increased further the second disorder-induced crumpling transition occurs. In contrast, for $\mathcal{T} > \mathcal{T}_*$, the crumpling transition happens before the stabilization of ripples. Our phase diagram suggests the possibility of a rippling transition with decreasing temperature at fixed disorder. The relevance of our theory for realistic membranes is also supported by numerical simulations [31] where the crumpling transition with increase of disorder was clearly seen. The phase diagram in Fig. 1 suggests that it is possible to probe all four phases by lowering the temperature at a given disorder. A very interesting subject for further research, we expect that the phase diagram is even more nontrivial in the case of long-range disorder [68].

Apart from fundamental importance, our results shed light on a temperature dependence of conductivity which is limited by scattering of carriers off the out-of-plane deformations [69]. For example, in the clean flat phase the conductivity of freestanding graphene is limited by flexural phonons and decays with T as $\sigma \propto T^{-\eta}\max\{(\mu/T)^{2-2\eta}, 1\}$, where μ is the Fermi level [62]. By contrast, in the rippled flat phase, the conductivity at $T \ll \mu$ saturates at a certain level, $\sigma = \text{const}$, which should strongly depend on localization effects similar to the scattering off a static disorder [70]. For $T \gg \mu$, there could exist an interval of temperatures in which the Drude-type approach is applied such that ripple-limited conductivity increases with temperature, $\sigma \propto T^{2-\eta'}$. A challenging problem is to study localization effects in the different

regions of our phase diagram due to scattering off out-of-plane fluctuations with emphasis on the regime of high-temperature localization predicted in Ref. [62].

As mentioned above, the clean and rippled flat phases can also be distinguished experimentally by measurement of the anomalous Hooke's law, $\varepsilon \sim F^{\alpha}$, where ε is the stretching caused by an applied stress F. In the clean and rippled flat phases, we have $\alpha = \eta/(2-\eta)$ [24] and $\alpha = \eta'_{\infty}/(2-\eta_{\infty})$, respectively.

To conclude, we predicted the phase diagram of a flexible 2D material (see Fig. 1). We demonstrated the existence of the crumpling- and rippling-transition lines, which cross each other at the multicritical point M. The rippling-transition line connects M with the singular stable point F, in which the rippled flat and clean flat phases coexist. Our results reconcile the theory of membrane elasticity with recent experimental and numerical data for disordered graphene.

ACKNOWLEDGMENTS

We thank I. Gornyi, I. Gruzberg, and A. Mirlin for fruitful discussions and M. Ben Shalom, Y. Gefen, and J. Schmalian for useful comments on the manuscript. The work was funded in part by the Alexander von Humboldt Foundation, by the Russian Ministry of Science and Higher Education, by the Basic Research Program of HSE, by Foundation for the Advancement of Theoretical Physics and Mathematics BASIS, and by the Russian Foundation for Basic Research (Grant No. 20-52-12019) – Deutsche Forschungsgemeinschaft (Grant No. SCHM 1031/12-1) cooperation. The authors are grateful to Karlsruhe Institute of Technology for hospitality.

APPENDIX A: SCREENED INTERACTION

The interaction between flexural phonons modifies the Green's function. The exact Green's function can be written as follows (in the replica limit $N \to 0$):

$$\hat{\mathcal{G}}(k) = T\left[\varkappa(1 - f\hat{J})k^4 - \hat{\Sigma}(k)\right]^{-1}. \tag{A1}$$

As is well known, before constructing the perturbation theory in the interaction between flexural phonons, it is important to take into account screening of this interaction by the flexural phonons themselves. This screening [see Fig. 2(b)] is determined by the bare polarization operator

$$\hat{\Pi}_{ab}(q) = \frac{d_c}{3T}\int_k \frac{[\boldsymbol{k}\times\boldsymbol{q}]^4}{q^4}\hat{\mathcal{G}}_{ab}(|\boldsymbol{k}-\boldsymbol{q}|)\hat{\mathcal{G}}_{ab}(k) = (1 + 2f + f^2\hat{J})\frac{d_c T}{16\pi\varkappa^2 q^2}. \tag{A2}$$

Here, we introduced for brevity the following shorthand notation: $\int_k \equiv \int d^2\boldsymbol{k}/(2\pi)^2$. Summation of the geometric series shown in Fig. 2(b) yields the screened interaction

$$\hat{N}(q) = \frac{\hat{Y}_q}{2} = \frac{Y_0/2}{1 + 3Y_0\hat{\Pi}(q)/2} = \frac{Y_0}{2}\frac{q^2}{q^2+\tilde{q}_*^2}\left(1 - \frac{f^2\hat{J}}{1+2f} + \frac{q^2}{q^2+\tilde{q}_*^2}\frac{f^2\hat{J}}{1+2f}\right). \tag{A3}$$

We mention that the screened interaction at small momenta $q \ll \tilde{q}_*$ becomes independent of the Young modulus Y_0 and proportional to $1/d_c$.

APPENDIX B: SELF-ENERGY CORRECTION

1. Contribution of the first order in $1/d_c$

The self-energy correction of the first order in $1/d_c$ is given by the diagram in Fig. 2(a). It can be written as

$$\hat{\Sigma}^{(1)}_{ab}(k) = -2\int_q \frac{[\boldsymbol{k}\times\boldsymbol{q}]^4}{q^4}\hat{N}_{ab}(q)\hat{\mathcal{G}}_{ab}(|\boldsymbol{k}-\boldsymbol{q}|) = -\frac{2}{d_c}\varkappa k^4\left[\frac{1+3f+f^2-f^3\hat{J}}{(1+2f)^2}L_0\left(\frac{k}{\tilde{q}_*}\right) + \frac{f^2(1+f\hat{J})}{(1+2f)^2}L_1\left(\frac{k}{\tilde{q}_*}\right)\right]_{ab}, \tag{B1}$$

where

$$L_m(K) = \int_0^{\infty}\frac{dq}{q}\frac{q^{2m}\min\{q^4/K^4, 1\}}{(1+q^2)^{m+1}}. \tag{B2}$$

For $m = 0, 1$ they are given explicitly as follows:

$$L_0(K) = -\ln K + \frac{1}{2}\ln(1+K^2) + \frac{K^2 - \ln(1+K^2)}{2K^4},$$
$$L_1(K) = \frac{K^2 - \ln(1+K^2)}{K^4}. \tag{B3}$$

In the limit $k/\tilde{q}_* \ll 1$ and $N \to 0$, we find

$$\hat{\Sigma}^{(1)}(k) = -\frac{2}{d_c}\varkappa k^4\left(\alpha_1\ln\frac{q_*}{k} - f\gamma_1\hat{J}\ln\frac{q'_*}{k}\right), \tag{B4}$$

where $q_* = \tilde{q}_*\exp[1/4 + \gamma_1/(2\alpha_1)]$ and $q'_* = \tilde{q}_*\exp(-1/4)$ and

$$\alpha_1 = \frac{1+3f+f^2}{(1+2f)^2}, \quad \gamma_1 = \frac{f^2}{(1+2f)^2}. \tag{B5}$$

2. Contribution of the second order in $1/d_c$

In this section we present results for the contribution of the second order in $1/d_c$ to the self-energy (see diagrams in Fig. 3).

a. Diagram in Fig. 3(a)

The contribution to the self-energy corresponding to the diagram in Fig. 3(a) has the following form:

$$\hat{\Sigma}^{(2,a)}_{ab}(k) = -\frac{2}{T}\int_q [\hat{\mathcal{G}}(|\boldsymbol{k}-\boldsymbol{q}|)\Sigma^{(1)}(|\boldsymbol{k}-\boldsymbol{q}|)\hat{\mathcal{G}}(|\boldsymbol{k}-\boldsymbol{q}|)]_{ab} \times\frac{[\boldsymbol{k}\times\boldsymbol{q}]^4}{q^4}\hat{N}_{ab}(q). \tag{B6}$$

Computing the integrals over momentum q in the same way as in Ref. [45], we obtain for $k/\tilde{q}_* \ll 1$ and

$N \to 0$

$$\hat{\Sigma}^{(2,a)}(k) = \frac{2}{d_c^2}\varkappa k^4\left\{\alpha^{(a)}\left[\ln^2\frac{q_*}{k} + \frac{1}{2}\ln\frac{q_*}{k}\right] + \tilde{\alpha}^{(a)}\ln\frac{q_*}{k} - f\hat{J}\left[\gamma^{(a)}\left(\ln^2\frac{q'_*}{k} + \frac{1}{2}\ln\frac{q'_*}{k}\right) + \tilde{\gamma}^{(a)}\ln\frac{q'_*}{k}\right]\right\}, \tag{B7}$$

where

$$\alpha^{(a)} = \frac{1+7f+16f^2+12f^3+f^4}{(1+2f)^4},$$
$$\gamma^{(a)} = \frac{f^2(2+6f+f^2)}{(1+2f)^4},$$
$$\tilde{\alpha}^{(a)} = -\frac{\gamma_1}{\beta_1}\beta^{(2,a)} + \frac{f^2(1+5f+5f^2)}{(1+2f)^4},$$
$$\tilde{\gamma}^{(a)} = \gamma^{(2,a)} + \frac{3f^4}{(1+2f)^4}. \tag{B8}$$

b. Diagram in Fig. 3(b)

The diagram in Fig. 3(b) can be considered as the first-order correction to the self-energy in which the interaction line is changed due to correction to the polarization operator:

$$\hat{\Sigma}^{(2,b)}_{ab} = \frac{6}{T}\int_q \frac{[\boldsymbol{k}\times\boldsymbol{q}]^4}{q^4}[\hat{N}(q)\delta\hat{\Pi}(q)\hat{N}(q)]_{ab}\hat{\mathcal{G}}_{ab}(|\boldsymbol{k}-\boldsymbol{q}|),$$
$$\delta\hat{\Pi}_{cd} = \frac{2d_c}{3T^2}\int_k \frac{[\boldsymbol{k}\times\boldsymbol{q}]^4}{q^4}\hat{\mathcal{G}}_{cd}(|\boldsymbol{k}-\boldsymbol{q}|)[\hat{\mathcal{G}}(k)\hat{\Sigma}^{(1)}(k)\hat{\mathcal{G}}(k)]_{cd}. \tag{B9}$$

The correction to the polarization operator can be computed as follows:

$$\delta\hat{\Pi}(q) = -\frac{T\delta\hat{\pi}(q/\tilde{q}_*)}{4\pi\varkappa^2 q^2}, \quad \delta\hat{\pi}(q) = \sum_{j=0,1}\delta\hat{\pi}_j\tilde{L}_j(q), \tag{B10}$$

where

$$\delta\hat{\pi}_0 = \frac{1+6f+10f^2+2f^3+f^2(2+6f+f^2)\hat{J}}{(1+2f)^2},$$
$$\delta\hat{\pi}_1 = \frac{f^2(1+4f+3f^2\hat{J})}{(1+2f)^2}, \tag{B11}$$

and

$$\tilde{L}_m(q) = \int_0^1 dk k L_m(kq) + \int_1^\infty \frac{dk}{k^3}L_m(kq). \tag{B12}$$

The functions $\tilde{L}_0$ and $\tilde{L}_1$ can be computed exactly as follows:

$$\tilde{L}_0(q) = \frac{(1+q^2)}{6q^2}\left[\frac{(1+q^2)^2}{q^2}\ln(1+q^2) - 1\right] - \frac{q^2+3}{3}\ln q,$$
$$\tilde{L}_1(q) = \frac{q^2}{3}\ln q - \frac{(q^2-2)}{6q^2}\left[\frac{(1+q^2)^2}{q^2}\ln(1+q^2) - 1\right]. \tag{B13}$$

Substituting the expression (B10) for the correction to the polarization operator into Eq. (B9), we obtain in the limits $k/\tilde{q}_* \ll 1$ and $N \to 0$

$$\hat{\Sigma}^{(2,b)}(k) = -\frac{4}{d_c^2}\varkappa k^4\left\{\alpha^{(b)}\left[\ln^2\frac{q_*}{k} + \frac{1}{2}\ln\frac{q_*}{k}\right] + \tilde{\alpha}^{(b)}\ln\frac{q_*}{k} - f\hat{J}\left[\gamma^{(b)}\left(\ln^2\frac{q'_*}{k} + \frac{1}{2}\ln\frac{q'_*}{k}\right) + \tilde{\gamma}^{(b)}\ln\frac{q'_*}{k}\right]\right\}, \tag{B14}$$

where

$$\alpha^{(b)} = \frac{1+9f+30f^2+42f^3+19f^4+2f^5}{(1+2f)^5},$$
$$\gamma^{(b)} = \frac{f^3(2+7f+2f^2)}{(1+2f)^5},$$
$$\tilde{\alpha}^{(b)} = -\frac{\gamma_1}{\beta}\beta^{(b)} + \frac{f^2(1+7f+15f^2+6f^3)}{(1+2f)^5},$$
$$\tilde{\gamma}^{(b)} = \gamma^{(b)} - \frac{f^4(1-2f)}{(1+2f)^5}. \tag{B15}$$

c. Diagram in Fig. 3(c)

The correction to the self-energy shown in Fig. 3(c) can be written as follows:

$$\hat{\Sigma}^{(2,c)}_{ab}(k) = \frac{4}{T}\int_{q,Q}\frac{[\boldsymbol{k}\times\boldsymbol{q}]^2}{q^2}\frac{[\boldsymbol{k}\times\boldsymbol{Q}]^2}{q^2}\frac{[(\boldsymbol{k}-\boldsymbol{q})\times\boldsymbol{Q}]^2}{Q^2} \times \frac{[(\boldsymbol{k}-\boldsymbol{Q})\times\boldsymbol{q}]^2}{q^2}\hat{\mathcal{G}}_{ac}(|\boldsymbol{k}-\boldsymbol{q}|)\hat{\mathcal{G}}_{cd}(|\boldsymbol{k}-\boldsymbol{Q}|) \times \hat{\mathcal{G}}_{db}(|\boldsymbol{k}-\boldsymbol{q}-\boldsymbol{Q}|)\hat{N}_{ad}(q)\hat{N}_{cb}(Q). \tag{B16}$$

Taking the integrals over momenta in the same way as in Ref. [45], we find in the limits $k/\tilde{q}_* \ll 1$ and $N \to 0$

$$\hat{\Sigma}^{(2,c)}(k) = \frac{7}{3d_c^2}\varkappa k^4(\alpha^{(c)} - f\gamma^{(c)}\hat{J})\ln\frac{q_*}{k}, \tag{B17}$$

where

$$\alpha^{(c)} = \frac{1+7f+17f^2+16f^3+5f^4}{(1+2f)^4},$$
$$\gamma^{(c)} = \frac{f^2(1+4f+f^2)}{(1+2f)^4}. \tag{B18}$$

d. Diagram in Fig. 3(d)

The correction to the self-energy shown in Fig. 3(d) can be written as follows:

$$\hat{\Sigma}^{(2,d)}_{ab}(k) = -\frac{4d_c}{T^2}\int_{Q,p,p'}\frac{[\boldsymbol{p}\times\boldsymbol{Q}]^2}{Q^2}\frac{[\boldsymbol{p}'\times\boldsymbol{Q}]^2}{Q^2}\frac{[\boldsymbol{p}\times\boldsymbol{p}']^2}{|\boldsymbol{p}-\boldsymbol{p}'|^2} \times \frac{[\boldsymbol{k}\times(\boldsymbol{p}-\boldsymbol{p}')]^4}{|\boldsymbol{p}-\boldsymbol{p}'|^4}\frac{[(\boldsymbol{p}-\boldsymbol{Q})\times(\boldsymbol{p}'-\boldsymbol{Q})]^2}{|\boldsymbol{p}-\boldsymbol{p}'|^2}\hat{N}_{lm}(Q) \times \hat{N}_{ac}(|\boldsymbol{p}-\boldsymbol{p}'|)\hat{N}_{bd}(|\boldsymbol{p}-\boldsymbol{p}'|)\hat{\mathcal{G}}_{cl}(p)\hat{\mathcal{G}}_{dl}(|\boldsymbol{p}-\boldsymbol{Q}|) \times \hat{\mathcal{G}}_{cm}(p')\hat{\mathcal{G}}_{dm}(|\boldsymbol{p}'-\boldsymbol{Q}|)\hat{\mathcal{G}}_{ab}(|\boldsymbol{k}-\boldsymbol{p}+\boldsymbol{p}'|). \tag{B19}$$

Integration over momenta can be performed in the same way as in Ref. [45]. Then for $k/\tilde{q}_* \ll 1$ and $N \to 0$ we

retrieve

$$\hat{\Sigma}^{(2,d)}(k) = -\frac{2}{d_c^2}\varkappa k^4(\alpha^{(d)} - f\gamma^{(d)}\hat{f})\ln\frac{q_*}{k}, \tag{B20}$$

where

$$\alpha^{(d)} = \frac{1+11f+49f^2+111f^3+130f^4+72f^5+16f^6}{(1+2f)^6},$$
$$\gamma^{(d)} = \frac{2f^4}{(1+2f)^5}. \tag{B21}$$

e. Diagram in Fig. 3(e)

The correction to the self-energy shown in Fig. 3(e) is as follows:

$$\hat{\Sigma}^{(2,e)}_{ab} = -\frac{8d_c}{T^2}\int_{q,p,Q}\frac{[\boldsymbol{k}\times\boldsymbol{q}]^2}{q^2}\frac{[\boldsymbol{k}\times\boldsymbol{Q}]^2}{Q^2}\frac{[\boldsymbol{p}\times\boldsymbol{q}]^2}{q^2}\frac{[\boldsymbol{p}\times\boldsymbol{Q}]^2}{Q^2}$$
$$\times\frac{[(\boldsymbol{k}-\boldsymbol{q})\times(\boldsymbol{Q}-\boldsymbol{q})]^2}{|\boldsymbol{q}-\boldsymbol{Q}|^2}\frac{[(\boldsymbol{p}-\boldsymbol{Q})\times(\boldsymbol{p}-\boldsymbol{q})]^2}{|\boldsymbol{q}-\boldsymbol{Q}|^2}$$
$$\times\hat{N}_{ac}(q)\hat{N}_{bd}(Q)\hat{N}_{lm}(|\boldsymbol{q}-\boldsymbol{Q}|)\hat{\mathcal{G}}_{cd}(p)\hat{\mathcal{G}}_{am}(|\boldsymbol{k}-\boldsymbol{q}|)$$
$$\times\hat{\mathcal{G}}_{mb}(|\boldsymbol{k}-\boldsymbol{Q}|)\hat{\mathcal{G}}_{cl}(|\boldsymbol{p}-\boldsymbol{q}|)\hat{\mathcal{G}}_{dl}(|\boldsymbol{p}-\boldsymbol{Q}|). \tag{B22}$$

Integration over momenta can be performed in the same way as in Ref. [45]. Then we obtain for $k/\tilde{q}_* \ll 1$ and $N \to 0$

$$\hat{\Sigma}^{(2,e)}(k) = -\frac{58}{27d_c^2}\varkappa k^4(\alpha^{(e)} - f\gamma^{(e)}\hat{f})\ln\frac{q_*}{k}, \tag{B23}$$

where

$$\alpha^{(e)} = \frac{1+11f+49f^2+111f^3+129f^4+67f^5+10f^6}{(1+2f)^6},$$
$$\gamma^{(e)} = \frac{2f^4(2+5f+2f^2)}{(1+2f)^6}. \tag{B24}$$

f. Diagram in Fig. 3(f)

The correction to the self-energy shown in Fig. 3(f) is given by the following explicit expression:

$$\hat{\Sigma}^{(2,f)}_{ab} = \frac{8d_c^2}{T^3}\int_{p,p',q,Q}\frac{[\boldsymbol{k}\times\boldsymbol{q}]^4}{q^4}\frac{[\boldsymbol{p}\times\boldsymbol{q}]^2}{q^2}\frac{[\boldsymbol{p}\times\boldsymbol{Q}]^2}{Q^2}\frac{[\boldsymbol{p}'\times\boldsymbol{Q}]^2}{Q^2}$$
$$\times\frac{[(\boldsymbol{p}-\boldsymbol{Q})\times(\boldsymbol{q}-\boldsymbol{Q})]^2}{|\boldsymbol{q}-\boldsymbol{Q}|^2}\frac{[(\boldsymbol{p}'-\boldsymbol{Q})\times(\boldsymbol{q}-\boldsymbol{Q})]^2}{|\boldsymbol{q}-\boldsymbol{Q}|^2}$$
$$\times\frac{[\boldsymbol{p}'\times\boldsymbol{q}]^2}{q^2}\hat{N}_{ac}(q)\hat{N}_{bd}(q)\hat{N}_{st}(|\boldsymbol{q}-\boldsymbol{Q}|)\hat{N}_{lm}(Q)$$
$$\times\hat{\mathcal{G}}_{cl}(p)\hat{\mathcal{G}}_{cs}(|\boldsymbol{p}-\boldsymbol{Q}|)\hat{\mathcal{G}}_{ls}(|\boldsymbol{p}-\boldsymbol{q}|)\hat{\mathcal{G}}_{dm}(p')$$
$$\times\hat{\mathcal{G}}_{dt}(|\boldsymbol{p}'-\boldsymbol{Q}|)\hat{\mathcal{G}}_{mt}(|\boldsymbol{p}'-\boldsymbol{q}|)\hat{\mathcal{G}}_{ab}(|\boldsymbol{k}-\boldsymbol{q}|). \tag{B25}$$

Integrating over momenta in the same way as in Ref. [45] and taking the limits $k/\tilde{q}_* \ll 1$ and $N \to 0$, we obtain

$$\hat{\Sigma}^{(2,f)}_{ab}(k) = \frac{3+68\zeta(3)}{27d_c^2}\varkappa k^4(\alpha^{(f)} - f\gamma^{(f)}\hat{f})\ln\frac{q_*}{k}, \tag{B26}$$

where

$$\alpha^{(f)} = \frac{1+11f+49f^2+111f^3+129f^4+64f^5+9f^6}{(1+2f)^6},$$
$$\gamma^{(f)} = \frac{f^4(1+6f+3f^2)}{(1+2f)^6}. \tag{B27}$$

g. Contribution of the second order in $1/d_c$

All in all, the six diagrams in Fig. 3 of the main text yield the following contribution to the self-energy in the second order in $1/d_c$:

$$\hat{\Sigma}^{(2)}(k) = -\frac{\alpha_2+2\tilde{\alpha}_2}{d_c^2}\ln\frac{q_*}{k} - \frac{2\alpha_2'}{d_c^2}\ln^2\frac{q_*}{k}$$
$$+ f\hat{f}\left[\frac{\gamma_2+2\tilde{\gamma}_2}{d_c^2}\ln\frac{q_*'}{k} + \frac{2\gamma_2'}{d_c^2}\ln^2\frac{q_*'}{k}\right], \tag{B28}$$

where

$$\alpha_2' = 2\alpha^{(b)} - \alpha^{(a)}, \quad \tilde{\alpha}_2 = 2\tilde{\alpha}^{(b)} - \tilde{\alpha}^{(a)},$$
$$\gamma_2' = 2\gamma^{(b)} - \gamma^{(a)}, \quad \tilde{\gamma}_2 = 2\tilde{\gamma}^{(b)} - \tilde{\gamma}^{(a)}, \tag{B29}$$

and

$$\alpha_2 = \alpha_2' - \frac{7}{3}\alpha^{(c)} + 2\alpha^{(d)} + \frac{58}{27}\alpha^{(e)} - \frac{3+68\zeta(3)}{27}\alpha^{(f)},$$
$$\gamma_2 = \gamma_2' - \frac{7}{3}\gamma^{(c)} + 2\gamma^{(d)} + \frac{58}{27}\gamma^{(e)} - \frac{3+68\zeta(3)}{27}\gamma^{(f)}. \tag{B30}$$

APPENDIX C: DERIVATION OF THE RG EQUATIONS

1. First order in $1/d_c$

The effect of the first-order correction (B4) to the self-energy can be interpreted as $1/d_c$ corrections to $\varkappa$ and f:

$$\varkappa(k) = \varkappa\left[1+\frac{2\alpha_1}{d_c}\ln\frac{q_*}{k}\right],$$
$$\varkappa(k)f(k) = \varkappa f\left[1+\frac{2\gamma_1}{d_c}\ln\frac{q_*'}{k}\right],$$
$$f(k) = f\left[1+\frac{2(\gamma_1-\alpha_1)}{d_c}\ln\frac{q_*''}{k}\right], \tag{C1}$$

where $q_*'' = \tilde{q}_* e^{1/4+\gamma_1/(\alpha_1-\gamma_1)}$. We mention that the perturbative results (C1) suggest that the bare parameters $\varkappa$ and f coincide with the renormalized parameters at the scales q_* and q_*'', respectively, i.e., $\varkappa \equiv \varkappa(q_*)$ and $f \equiv f(q_*'')$. Also we note that the following relation holds: $\varkappa(q_*)f(q_*'') = \varkappa(q_*')f(q_*')$.

The perturbative corrections (C1) can be recast in the form of the RG equations [29,35]:

$$-\frac{d\ln\varkappa}{d\ln k} = \frac{\eta_\varkappa^{(1)}}{d_c}, \quad -\frac{d\ln f}{d\ln k} = \frac{\beta^{(1)}}{d_c},$$
$$\eta_\varkappa^{(1)} = 2\alpha_1, \quad \beta^{(1)} = 2(\gamma_1-\alpha_1). \tag{C2}$$

Since the momentum scales are arranged as $q_*' < q_* < q_*''$, strictly speaking, the RG equations (C2) are valid for $k < q_*'$.

2. Second order in $1/d_c$

The results (B4) and (B28) for the self-energy allow us to write the following perturbative expansions for bending rigidity $\varkappa$ and the parameter f:

$$\frac{\varkappa(k)}{\varkappa(q_*)} = 1 + \frac{2\alpha_1}{d_c}\ln\frac{q_*}{k} + \frac{1}{d_c^2}\left(\alpha_2 + 4f\gamma_1\frac{d\alpha_1}{df}\ln\frac{q'_*}{q_*}\right)\ln\frac{q_*}{k}, + \frac{2}{d_c^2}\left[\alpha_1^2 + (\gamma_1-\alpha_1)f\frac{d\alpha_1}{df}\right]\ln^2\frac{q_*}{k} \tag{C3}$$

$$\frac{f(k)}{f(q''_*)} = 1 + \left(\frac{2(\gamma_1-\alpha_1)}{d_c} + \frac{(\gamma_2-\alpha_2)}{d_c^2}\right)\ln\frac{q''_*}{k} + \frac{2(\gamma_1-\alpha_1)}{d_c^2}\frac{d[f(\gamma_1-\alpha_1)]}{df}\ln^2\frac{q''_*}{k}. \tag{C4}$$

We emphasize that f in the right-hand side of Eqs. (C3) and (C4) is defined at the momentum scale q''_*. Also we note that in derivation of Eqs. (C3) and (C4) we used the following nontrivial relations:

$$\alpha'_2 = \alpha_1^2 + (\gamma_1-\alpha_1)f\frac{d\alpha_1}{df}, \quad \gamma'_2 = \gamma_1^2 + (\gamma_1-\alpha_1)f\frac{d\gamma_1}{df}. \tag{C5}$$

The perturbative expansion (C4) describes how the disorder parameter f transforms under a change of the momentum scale from q''_* to k. The form of Eq. (C3) is a bit unconventional since its right-hand side involves f not at the momentum scale q_* but at another momentum scale, q''_*. Therefore it is convenient to rewrite Eq. (C3) with f defined at the momentum scale q_* in its right-hand side:

$$\frac{\varkappa(k)}{\varkappa(q_*)} = 1 + \left(\frac{2\alpha_1}{d_c} + \frac{\alpha_2}{d_c^2}\right)\ln\frac{q_*}{k} + \frac{2}{d_c^2}\left[\alpha_1^2 + (\gamma_1-\alpha_1)f\frac{d\alpha_1}{df}\right]\ln^2\frac{q_*}{k}. \tag{C6}$$

We stress that f in the right-hand side of Eq. (C6) is defined at the momentum scale q_*.

The results (C4) and (C6) can be cast from perturbative solutions of the following RG equations for $\varkappa$ and f:

$$-\frac{d\ln\varkappa}{d\ln k} = \eta_\varkappa = \frac{\eta_\varkappa^{(1)}}{d_c} + \frac{\eta_\varkappa^{(2)}}{d_c^2}, \quad -\frac{d\ln f}{d\ln k} = \beta(f) = \frac{\beta^{(1)}}{d_c} + \frac{\beta^{(2)}}{d_c^2}, \tag{C7}$$

where $\eta_\varkappa^{(2)} = \alpha_2$ and $\beta^{(2)} = \alpha_2 - \gamma_2$. The coefficients $\eta_\varkappa^{(1)}$ and $\eta_\varkappa^{(2)}$ are given by Eqs. (5) and (6), respectively. For convenience, we present the final expressions for the first- and second-order coefficients of $\beta(f)$,

$$\beta^{(1)} = -\frac{2(1+3f)}{(1+2f)^2} \tag{C8}$$

and

$$\beta^{(2)} = -[73+803f+3667f^2+8517f^3+9278f^4+3420f^5 + 186f^6 - 68\zeta(3)(1+11f+49f^2+111f^3 + 128f^4+58f^5+6f^6)]/[27(1+2f)^6]. \tag{C9}$$

[1] K. S. Novoselov, A. K. Geim, S. V. Morozov, D. Jiang, Y. Zhang, S. V. Dubonos, I. V. Grigorieva, and A. A. Firsov, Electric field effect in atomically thin carbon films, Science **306**, 666 (2004).

[2] K. S. Novoselov, A. K. Geim, S. V. Morozov, D. Jiang, M. I. Katsnelson, I. V. Grigorieva, S. V. Dubonos, and A. A. Firsov, Two-dimensional gas of massless Dirac fermions in graphene, Nature (London) **438**, 197 (2005).

[3] Y. Zhang, Y.-W. Tan, H. L. Stormer, and P. Kim, Experimental observation of the quantum Hall effect and Berry's phase in graphene, Nature (London) **438**, 201 (2005).

[4] K. S. Novoselov and A. H. Castro Neto, Two-dimensional crystals-based heterostructures: Materials with tailored properties, Phys. Scr. **2012**, 014006 (2012).

[5] A. K. Geim and K. S. Novoselov, The rise of graphene, Nat. Mater. **6**, 183 (2007).

[6] K. S. Novoselov, Z. Jiang, Y. Zhang, S. V. Morozov, H. L. Stormer, U. Zeitler, J. C. Maan, G. S. Boebinger, P. Kim, and A. K. Geim, Room-temperature quantum Hall effect in graphene, Science **315**, 1379 (2007).

[7] A. H. Castro Neto, F. Guinea, N. M. R. Peres, K. S. Novoselov, and A. K. Geim, The electronic properties of graphene, Rev. Mod. Phys. **81**, 109 (2009).

[8] S. Das Sarma, S. Adam, E. H. Hwang, and E. Rossi, Electronic transport in two-dimensional graphene, Rev. Mod. Phys. **83**, 407 (2011).

[9] V. N. Kotov, B. Uchoa, V. M. Pereira, F. Guinea, and A. H. Castro Neto, Electron-electron interactions in graphene: Current status and perspectives, Rev. Mod. Phys. **84**, 1067 (2012).

[10] M. I. Katsnelson, *Graphene: Carbon in Two Dimensions* (Cambridge University Press, Cambridge, 2012).

[11] E. L. Wolf, *Graphene: A New Paradigm in Condensed Matter and Device Physics* (Oxford University Press, Oxford, 2014).

[12] L. E. F. Foa Torres, S. Roche, and J.-C. Charlier, *Introduction to Graphene-Based Nanomaterials: From Electronic Structure to Quantum Transport* (Cambridge University Press, Cambridge, 2014).

[13] H. Zhang, Ultrathin two-dimensional nanomaterials, ACS Nano **9**, 9451 (2015).

[14] *Fundamentals and Sensing Applications of 2D Materials*, edited by C. S. Rout, D. J. Late, and M. Hywel, Woodhead Publishing Series in Electronic and Optical Materials (Woodhead Publishing, Duxford, 2019).

[15] G. Fiori, F. Bonaccorso, G. Iannaccone, T. Palacios, D. Neumaier, A. Seabaugh, S. K. Banerjee, and L. Colombo, Electronics based on two-dimensional materials, Nat. Nanotechnol. **9**, 768 (2014).

[16] G. Iannaccone, F. Bonaccorso, L. Colombo, and G. Fiori, Quantum engineering of transistors based on 2D materials heterostructures, Nat. Nanotechnol. **13**, 183 (2018).

[17] Z. Dai, L. Liu, and Z. Zhang, Strain engineering of 2D materials: Issues and opportunities at the interface, Adv. Mater. **31**, 1805417 (2019).

[18] G. Wang, Z. Dai, J. Xiao, S. Feng, C. Weng, L. Liu, Z. Xu, R. Huang, and Z. Zhang, Bending of Multilayer van der Waals Materials, Phys. Rev. Lett. **123**, 116101 (2019).

[19] D. Nelson and L. Peliti, Fluctuations in membranes with crystalline and hexatic order, J. Phys. (Paris) **48**, 1085 (1987).

[20] J. A. Aronovitz and T. C. Lubensky, Fluctuations of Solid Membranes, Phys. Rev. Lett. **60**, 2634 (1988).

[21] M. Paczuski, M. Kardar, and D. R. Nelson, Landau Theory of the Crumpling Transition, Phys. Rev. Lett. **60**, 2638 (1988).

[22] F. David and E. Guitter, Crumpling transition in elastic membranes: Renormalization group treatment, Europhys. Lett. **5**, 709 (1988).

[23] E. Guitter, F. David, S. Leibler, and L. Peliti, Crumpling and Buckling Transitions in Polymerized Membranes, Phys. Rev. Lett. **61**, 2949 (1988).

[24] J. Aronovitz, L. Golubovic, and T. C. Lubensky, Fluctuations and lower critical dimensions of crystalline membranes, J. Phys. (Paris) **50**, 609 (1989).

[25] E. Guitter, F. David, S. Leibler, and L. Peliti, Thermodynamical behavior of polymerized membranes, J. Phys. (Paris) **50**, 1787 (1989).

[26] D. C. Morse, T. C. Lubensky, and G. S. Grest, Quenched disorder in tethered membranes, Phys. Rev. A **45**, R2151 (1992).

[27] D. R. Nelson and L. Radzihovsky, Polymerized membranes with quenched random internal disorder, Europhys. Lett. **16**, 79 (1991).

[28] L. Radzihovsky and D. R. Nelson, Statistical mechanics of randomly polymerized membranes, Phys. Rev. A **44**, 3525 (1991).

[29] D. C. Morse and T. C. Lubensky, Curvature disorder in tethered membranes: A new flat phase at $T = 0$, Phys. Rev. A **46**, 1751 (1992).

[30] D. Bensimon, D. Mukamel, and L. Peliti, Quenched curvature disorder in polymerized membranes, Europhys. Lett. **18**, 269 (1992).

[31] I. Giordanelli, M. Mendoza, J. S. Andrade Jr., M. A. F. Gomes, and H. J. Herrmann, Crumpling damaged graphene, Sci. Rep. **6**, 25891 (2016).

[32] R. J. T. Nicholl, H. J. Conley, N. V. Lavrik, I. Vlassiouk, Y. S. Puzyrev, V. P. Sreenivas, S. T. Pantelides, and K. I. Bolotin, The effect of intrinsic crumpling on the mechanics of free-standing graphene, Nat. Commun. **6**, 8789 (2015).

[33] R. J. T. Nicholl, N. V. Lavrik, I. Vlassiouk, B. R. Srijanto, and K. I. Bolotin, Hidden Area and Mechanical Nonlinearities in Freestanding Graphene, Phys. Rev. Lett. **118**, 266101 (2017).

[34] J. H. Los, A. Fasolino, and M. I. Katsnelson, Scaling Behavior and Strain Dependence of In-Plane Elastic Properties of Graphene, Phys. Rev. Lett. **116**, 015901 (2016).

[35] I. V. Gornyi, V. Yu. Kachorovskii, and A. D. Mirlin, Rippling and crumpling in disordered free-standing graphene, Phys. Rev. B **92**, 155428 (2015).

[36] P. Le Doussal and L. Radzihovsky, Anomalous elasticity, fluctuations and disorder in elastic membranes, Ann. Phys. (NY) **392**, 340 (2018).

[37] I. V. Gornyi, V. Yu. Kachorovskii, and A. D. Mirlin, Anomalous Hooke's law in disordered graphene, 2D Mater. **4**, 011003 (2017).

[38] S. Yeo, J. Han, S. Bae, and D. S. Lee, Coherence in defect evolution data for the ion beam irradiated graphene, Sci. Rep. **8**, 13973 (2018).

[39] H. Li, L. Daukiya, S. Haldar, A. Lindblad, B. Sanyal, O. Eriksson, D. Aubel, S. Hajjar-Garreau, L. Simon, and K. Leifer, Site-selective local fluorination of graphene induced by focused ion beam irradiation, Sci. Rep. **6**, 19719 (2016).

[40] D. Yllanes, S. S. Bhabesh, D. R. Nelson, and M. J. Bowick, Thermal crumpling of perforated two-dimensional sheets, Nat. Commun. **8**, 1381 (2017).

[41] L. Radzihovsky and P. Le Doussal, Crumpled glass phase of randomly polymerized membranes in the large d limit, J. Phys. I (France) **2**, 599 (1992).

[42] This situation corresponds to a 2D membrane embedded in a space of $d_c + 2$ dimensions. Although in the physical case $d_c = 1$, the large-d_c expansion captures basic physics of membranes and allows us to describe analytically the crumpling transition [22].

[43] I. S. Burmistrov, I. V. Gornyi, V. Yu. Kachorovskii, M. I. Katsnelson, J. H. Los, and A. D. Mirlin, Stress-controlled Poisson ratio of a crystalline membrane: Application to graphene, Phys. Rev. B **97**, 125402 (2018).

[44] I. S. Burmistrov, V. Yu. Kachorovskii, I. V. Gornyi, and A. D. Mirlin, Differential Poisson's ratio of a crystalline two-dimensional membrane, Ann. Phys. (NY) **396**, 119 (2018).

[45] D. R. Saykin, I. V. Gornyi, V. Yu. Kachorovskii, and I. S. Burmistrov, Absolute Poisson's ratio and the bending rigidity exponent of a crystalline two-dimensional membrane, Ann. Phys. (NY) **414**, 168108 (2020).

[46] P. Le Doussal and L. Radzihovsky, Self-consistent Theory of Polymerized Membranes, Phys. Rev. Lett. **69**, 1209 (1992).

[47] D. Gazit, Structure of physical crystalline membranes within the self-consistent screening approximation, Phys. Rev. E **80**, 041117 (2009).

[48] J.-P. Kownacki and D. Mouhanna, Crumpling transition and flat phase of polymerized phantom membranes, Phys. Rev. E **79**, 040101 (2009).

[49] F. L. Braghin and N. Hasselmann, Thermal fluctuations of free-standing graphene, Phys. Rev. B **82**, 035407 (2010).

[50] O. Coquand, K. Essafi, J.-P. Kownacki, and D. Mouhanna, Glassy phase in quenched disordered crystalline membranes, Phys. Rev. E **97**, 030102(R) (2018).

[51] G. Lopez-Polin, C. Gomez-Navarro, V. Parente, F. Guinea, M. I. Katsnelson, F. Perez-Murano, and J. Gomez-Herrero, Increasing the elastic modulus of graphene by controlled defect creation, Nat. Phys. **11**, 26 (2015).

[52] G. Lopez-Polin, M. Jaafar, F. Guinea, R. Roldan, C. Gomez-Navarro, and J. Gomez-Herrero, The influence of strain on the elastic constants of graphene, Carbon **124**, 42 (2017).

[53] K. V. Zakharchenko, M. I. Katsnelson, and A. Fasolino, Finite Temperature Lattice Properties of Graphene beyond the Quasiharmonic Approximation, Phys. Rev. Lett. **102**, 046808 (2009).

[54] W. Bao, F. Miao, Z. Chen, H. Zhang, W. Jang, C. Dames, and C. N. Lau, Controlled ripple texturing of suspended graphene and ultrathin graphite membranes, Nat. Nanotechnol. **4**, 562 (2009).

[55] D. Yoon, Y.-W. Son, and H. Cheong, Negative thermal expansion coefficient of graphene measured by Raman spectroscopy, Nano Lett. **11**, 3227 (2011).

[56] P. L. de Andres, F. Guinea, and M. I. Katsnelson, Bending modes, anharmonic effects, and thermal expansion coefficient in single-layer and multilayer graphene, Phys. Rev. B **86**, 144103 (2012).

[57] A. L. C. da Silva, L. Cândido, J. N. Teixeira Rabelo, G.-Q. Hai, and F. M. Peeters, Anharmonic effects on thermodynamic properties of a graphene monolayer, Europhys. Lett., **107**, 56004 (2014).

[58] K. H. Michel, S. Costamagna, and F. M. Peeters, Theory of anharmonic phonons in two-dimensional crystals, Phys. Rev. B **91**, 134302 (2015).

[59] I. S. Burmistrov, I. V. Gornyi, V. Yu. Kachorovskii, M. I. Katsnelson, and A. D. Mirlin, Quantum elasticity of graphene: Thermal expansion coefficient and specific heat, Phys. Rev. B **94**, 195430 (2016).

[60] K. I. Bolotin, K. J. Sikes, J. Hone, H. L. Stormer, and P. Kim, Temperature-Dependent Transport in Suspended Graphene, Phys. Rev. Lett. **101**, 096802 (2008).

[61] E. V. Castro, H. Ochoa, M. I. Katsnelson, R. V. Gorbachev, D. C. Elias, K. S. Novoselov, A. K. Geim, and F. Guinea, Limits on Charge Carrier Mobility in Suspended Graphene due to Flexural Phonons, Phys. Rev. Lett. **105**, 266601 (2010).

[62] I. V. Gornyi, V. Yu. Kachorovskii, and A. D. Mirlin, Conductivity of suspended graphene at the Dirac point, Phys. Rev. B **86**, 165413 (2012).

[63] We note that analysis of the structure of the higher order in $1/d_c$ diagrams suggests that the corrections to the position of the unstable fixed point are $O(1/d_c)$ and thus are negligible at $d_c \gg 1$.

[64] Recently, an unstable fixed point similar to f_* has been found for a disordered membrane of $D = 4 - \epsilon$ dimension within the second-order expansion in ϵ and for a 2D disordered membrane within the analytically uncontrolled nonperturbative renormalization group (NPRG) approach [50].

[65] H. Nishimori, *Statistical Physics of Spin Glasses and Information Processing: An Introduction* (Clarendon Press, Oxford, 2001).

[66] P. Le Doussal and A. B. Harris, Location of the Ising Spin-Glass Multicritical Point on Nishimori's Line, Phys. Rev. Lett. **61**, 625 (1988).

[67] D. R. Saykin, V. Yu. Kachorovskii, and I. S. Burmistrov (unpublished).

[68] P. Le Doussal and L. Radzihovsky, Flat glassy phases and wrinkling of polymerized membranes with long-range disorder, Phys. Rev. B **48**, 3548 (1993).

[69] See Ref. [62] and references therein.

[70] P. M. Ostrovsky, I. V. Gornyi, and A. D. Mirlin, Electron transport in disordered graphene, Phys. Rev. B **74**, 235443 (2006).